ISSN 2087-3336 (Print) | 2721-4729 (Online)
TEKNOSAINS: Jurnal Sains, Teknologi dan Informatika
Vol. 12, No. 2, 2025, page. 227-234
http://jurnal.sttmcileungsi.ac.id/index.php/tekno
https://doi.org/10.37373/tekno.v12i2

Characteristics of two-phase flow patterns of non-Newtonian fluid xanthan gum-nitrogen in a horizontal square microchannel at high temperature

Ahmad Yusuf Ramadhan*, Haslinda Kusumaningsih, Deendarliyanto

*Universitas Gadjah Mada, Jl. Grafika No. 2. Yogyakarta, Indonesia 55281

* Corresponding Author: ahmadyusuframadhan1398@mail.ugm.ac.id

Submitted: 07/01/2025 Revised: 24/04/2025 Accepted: 11/05/2025

ABSTRACT

The development of microfluidic systems in the microscale requires a deep understanding of the characteristics of two-phase flow, especially when involving non-Newtonian fluids such as Xanthan Gum (XG) solution. This study aims to examine the flow patterns, transitions between patterns, and frictional pressure drop in two-phase flows of XG-Nitrogen and Aquades-Nitrogen in a square-shaped horizontal microchannel at high temperatures. The methods used include an experimental approach with high-speed camera visualization and pressure measurements, as well as numerical analysis using a two-phase pressure drop prediction model. The experimental results show three main flow patterns, namely slug, churn, and slug-annular, with the absence of bubbly and wavy-annular patterns in the XG flow, indicating the strong influence of non-Newtonian viscosity. The flow pattern transition occurs with increasing gas flow rate, causing changes in the slug shape. The evaluation of the prediction model shows better accuracy in 0.2% XG solution compared to Aquades, although there is still a deviation at high values. This study confirms the importance of non-Newtonian fluid viscosity on flow stability and frictional stress, and contributes to the design of more efficient microcooling systems.

Keyword: Xanthan gum; aquades; nitrogen; aliran dua fase; viskositas non-newtonian

1. INTRODUCTION

The use of microfluidic systems in recent decades has grown rapidly, especially in the fields of chemical engineering, pharmaceuticals, and electronic cooling [1]. One of the innovations in microchannels is the implementation of gas-liquid two-phase flow, which offers significant thermal efficiency and heat transfer enhancements for a variety of micro-scale applications [2].

Gas-liquid two-phase flow in square-shaped horizontal microchannels presents its challenges, mainly due to the complex flow patterns and instabilities that arise when using non-Newtonian fluids such as xanthan gum, which has viscoelastic properties [3][4]. At high temperature conditions, the viscosity and pseudo-plastic characteristics of xanthan gum as a non-Newtonian fluid play an important role in determining the flow pattern and pressure drop in microchannels [5].

Research shows that rheological factors such as shear stress and viscosity greatly influence the flow behavior, as well as the transition pattern from slug to annular flow in microchannels with narrow geometry [6][7]. The study of non-Newtonian two-phase flow patterns at high temperatures aims to improve understanding of heat transfer characteristics and flow stability in square-shaped microchannels [8][9].

Experiments using high-speed visualization and pressure analysis will be conducted to identify flow patterns, transition points between patterns, and hydrodynamic resistance characteristics in

rectangular horizontal channels [10]. This research is expected to provide more in-depth guidance for the development of micro cooling system designs and other micro engineering applications [11].

Test Fluid: In this study, distilled water and Xanthan Gum (XG) with a concentration of 0.2 wt% were used. XG solution was made by mixing distilled water and XG powder according to the specified weight ratio until homogeneously mixed [12]. This XG solution provides non-Newtonian fluid characteristics, and the relationship between apparent viscosity and shear rate can be expressed by equation (1).

$$\mu_a = k\left(\frac{du}{dy}\right)^{n-1} \tag{1}$$

Where du/dy is the shear rate, μα is the apparent viscosity, k is the consistency coefficient, and nnn is the flow index. To determine the magnitude of apparent viscosity in non-Newtonian fluids, the equation proposed used [13] was used. For a square cross section, the values a = 0.2121 and b = 0.6766. Shown in Eq (6).

$$\mu_\alpha = k(\frac{\alpha+bn}{n})^n\,(\frac{8j_L}{D}) \tag{2}$$

Table 1 shows the properties of the test fluids used, which were obtained from secondary data from previous studies [12].

Table 1. Working fluid properties

Fluid	Surface Tension σ (N/m)	Density (kg/m³)	K (Pa.sⁿ)	n
Air	0.07269	998.5	0.00097	1.00
XG 0,2 wt%	0.07335	1006	0.029	0.73

Working Fluid Properties: This study uses several equations to identify the characteristics of fluid flow. The following is an explanation of some of the properties used. The superficial velocity of liquid and gas is calculated using equation (3).

$$j_G = \frac{Q_G}{A}\ j_L = \frac{Q_L}{A} \tag{3}$$

Where Q is the flow rate, which is mass per unit time, and A is the cross-sectional area of the channel.

The friction factor for single-phase laminar flow in a rectangular channel can be calculated by utilizing the equation proposed [14], which is a function of the aspect ratio λ. Therefore, the friction factor can be calculated using equation (4).

$$f = 96(1 - 1{,}3353\lambda^2 - 1{,}7012\lambda^2 + 0{,}9564\lambda^4 - 0{,}2537\lambda^5)/R_e \tag{4}$$

The Reynolds number (Re) for Newtonian fluids is calculated using equation (5), while for non-Newtonian fluids it is defined through equation (6).

$$Re_G = \frac{\rho_G\, j_G D_H}{\mu_G}\ Re_L = \frac{\rho_L\, j_L D_H}{\mu_L} \tag{5}$$

$$Re'_L = \frac{8^{1-n} D_H{}^n \rho_l J_L{}^{2-n}}{k}\left(\frac{n}{a+bn}\right)^n \tag{6}$$

In addition, this study also takes into account the Weber Number and Bond Number. Both numbers can be calculated using equations (7) and (8).

$$We_G = \frac{\rho_G\, J_G{}^2 D_H}{\mu_G}\ We_L = \frac{\rho_L\, J_L D_H}{\mu_L} \tag{7}$$

$$Bo = \frac{(\rho_L - \rho_G)\, j_L D_H}{\mu_\alpha} \tag{8}$$

Coefficient C: The coefficient C is a constant that characterizes the interaction between two phases, and its value is very dependent on the nature of the flow, whether laminar or turbulent, which is determined by the Reynolds number proposed a constant value of C based on the test data they obtained [15], as stated in Equation (9), while propose different values of the constant C which are addressed in equation (10) [16][17].

$$C = 1{,}38Bo^{0,04}Re_L^{0,25}We_G^{-0,12} \quad (9)$$

$$C = 21(1\text{-}e^{-0.316D_h}) \quad (10)$$

2. METHOD

The sequence of research methodology is a description of the research design that will be carried out. Figure *1* shows an illustration of the planned research stages.

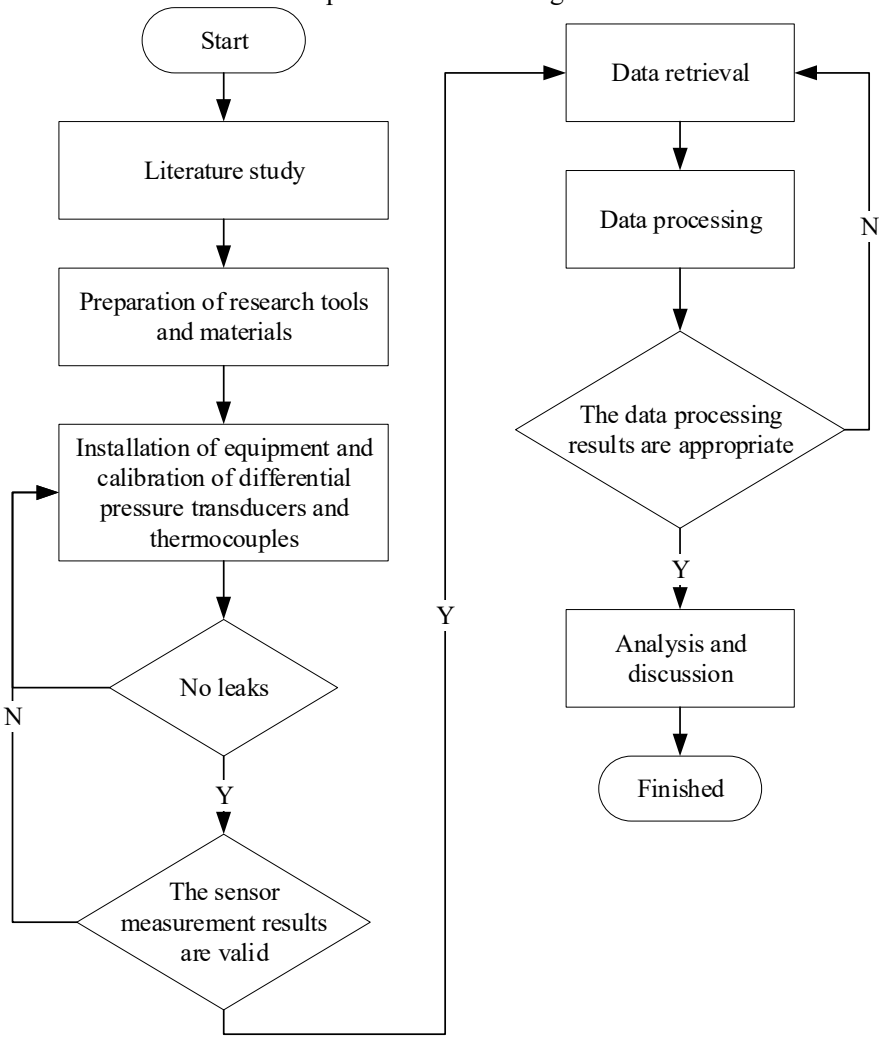

Figure 1. Research flow diagram

Figure 2 shows a schematic diagram of the equipment and details of the microfluidic chip used in the microchannel research facility. The microfluidic chip has a square cross-section with a side length of 0.8 mm and is equipped with 8 holes. There are 2 inlets, where the gas inlet will be the nitrogen injection hole, and the liquid inlet will be the fluid injection hole. Numbers 3 and 4 are used to measure the pressure drop by connecting them to the differential pressure transducer. Number 5 will be used for the thermocouple used to measure the wall temperature. Number 6 will be the outlet.

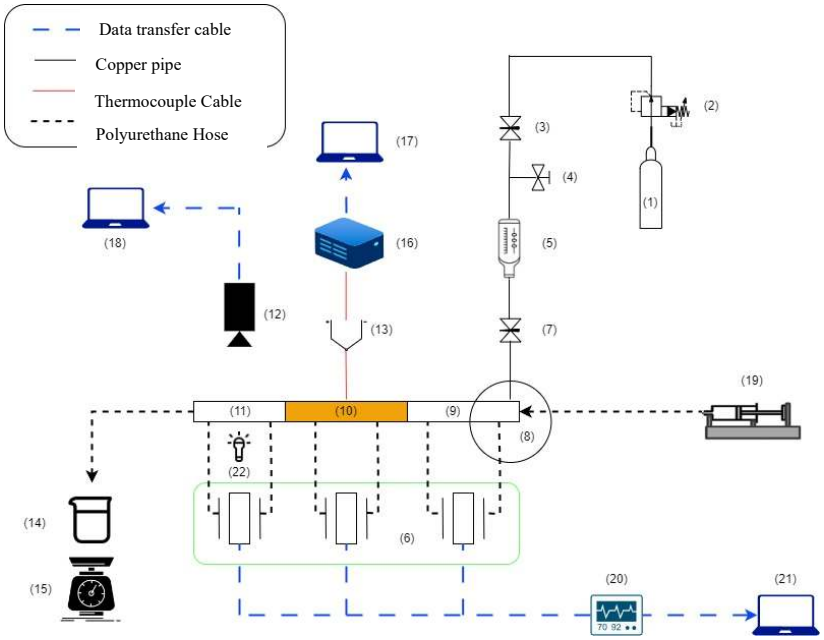

Figure 2. Schematic diagram of research apparatus and micro-fluidic chip

Nitrogen gas is injected from a nitrogen cylinder and flows through a copper pipe. A nitrogen gas flowmeter is used to regulate the gas flow rate. The liquid fluid will be injected into the microfluidic chip using a syringe pump, which will then push the fluid according to the JL required during the experiment. The fluid will then enter a heater, which has a temperature of approximately 40-45 degrees C. To validate that the liquid fluid (JL) and gas (JG) flow rates are by the target, the liquid fluid coming out of the microfluidic chip is collected and weighed using a Sartorius Quintix224-1S precision scale, which has a capacity of 220 grams and an accuracy of 0.0001 grams.

Visualize the flow patterns that occur, a high-speed camera Phantom Miro S310 is used in the observation area with a resolution of 384 x 288 pixels and a sampling rate of 25,000 fps. LED lights are placed directly under the microfluidic chip as a lighting medium.

3. RESULTS AND DISCUSSION

A. Flow Pattern

Two-phase flow patterns were identified in the observation area, located between two pressure taps (Z = 40 mm), to ensure that the flow that occurs is fully developed. In the Air-Nitrogen and XG-Nitrogen flows, the flow patterns formed include slug, slug-annular, and churn see Figure 3 and Figure 4. Figure 5 shows the results of the flow patterns formed in aquades fluid and XG 0.2% with JG 0.26 and JL 0.1, where the resulting flow pattern is in the form of a Slug. Relevant documentation to answer the research objectives is presented. Observations were made with a high-speed camera with a resolution of 512x384 pixels with a capture speed of 500 fps, which recorded three typical flow patterns, namely slug flow (S), churn flow (C), and slug-annular flow (SA).

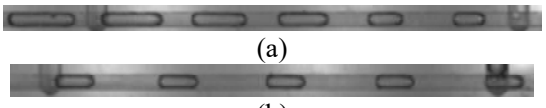

(a)

(b)

Figure 3. Slug flow patterns formed at JG 0.26 and JL 0.05 (a) Aquades, (b) XG 0.2%

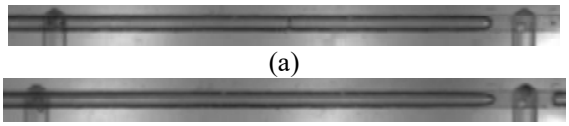

(a)

(b)

Figure 4. Slug-annular flow pattern formed at JG 1.04 and JL 0.1 (a) Aquades, (b) XG 0.2%

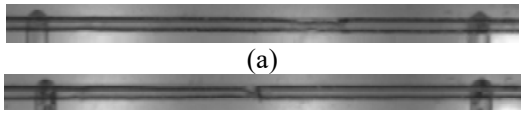

(a)

(b)

Figure 5. Churn flow pattern formed at JG 5.21 and JL 0.5 (a) Aquades, (b) XG 0.2%

B. Flow pattern regime

Figure 6 shows the flow regime maps for both test fluids, both Newtonian and non-Newtonian. In the figure, the black lines indicate the transition boundaries and flow regimes. Straight lines are used to distinguish flow patterns because the changes at the transition boundaries are very small, compared to the slanted lines or curves that show the general trend. The flow patterns identified in both test fluids are mostly similar. In addition, there is a significant change at the transition from slug to churn flow for different liquid fluids.

The flow pattern transition from slug to slug-annular occurs when JG is increased. This causes the gas phase filling the channel to increase, so that the slug length also increases. In fact, at some times, the gas phase in one frame is not interrupted. However, in general, the flow pattern formed is slug-annular, where the annular flow pattern is often interrupted by necking. In the Air-Nitrogen flow, the transition from slug to slug-annular flow pattern is interspersed with wavy-annular flow patterns, which are characterized by long annular flow with continuous necking waves without breaking the gas phase.

The transition from slug to churn flow pattern is accompanied by a slug-churn flow pattern. This transition is identified by the emergence of slug and churn flow patterns in one phenomenon. In the slug nose and slug tail, there are dispersed bubbles, but the boundary between the slugs is still clearly visible. Meanwhile, the transition from slug-churn to churn flow pattern is marked by the disappearance of the slug boundary in one phenomenon. The churn flow pattern tends to have long flow characteristics that are sometimes interrupted by dispersed bubbles.

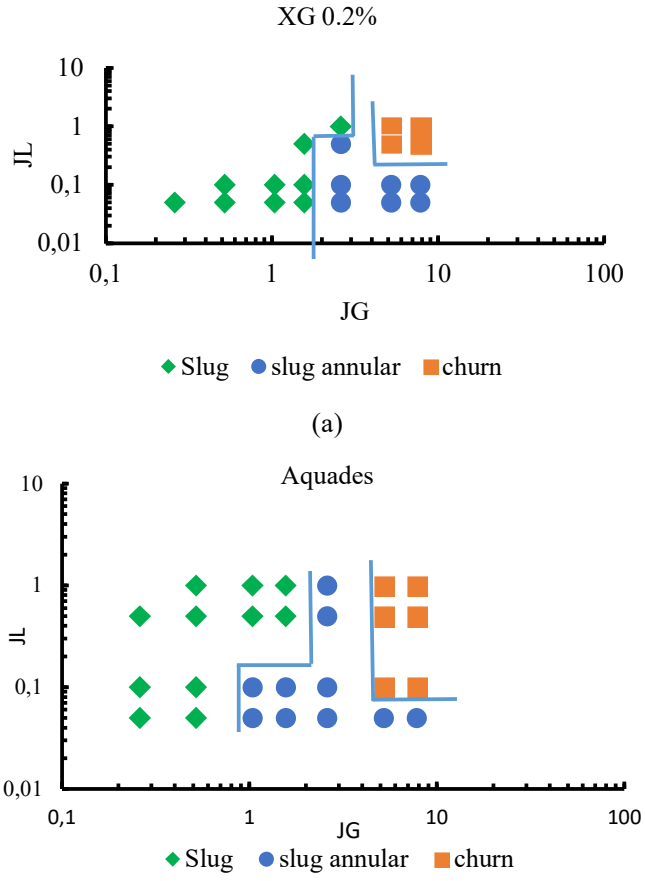

Figure 6. Flow pattern map (a) XG 0.2%, (b) Aquades

C. Evaluation of pressure drop correlation

Correlations based on homogeneous and separated flow models are often used to estimate the two-phase pressure drop. In the homogeneous flow model, the two-phase flow is considered as a single-phase flow with homogeneous characteristics, and the friction pressure drop gradient is expressed in Equation (15).

$$\left(\frac{dp_f}{dZ}\right)_{TP} = \phi_L^2 \left(\frac{dp_f}{dZ}\right)_L \quad (15)$$

ϕ_L^2 is the two-phase friction multiplier, which must be calculated using the method proposed by [7] shown in equation (16).

$$\phi_L^2 = 1 + \frac{C}{X} + \frac{1}{X^2} \quad (16)$$

Where X is the Martinelli parameter defined as equation (17).

$$X^2 = \frac{\left(\frac{dp_f}{dZ}\right)_L}{\left(\frac{dp_f}{dZ}\right)_G} \quad (17)$$

Calculate the error value in the frictional pressure drop data from the experimental results against the previously existing empirical equation. The method used involves Equations (18) and (19). These equations determine the mean-absolute-percentage error and root-mean-square-percentage error as error indicators.

$$E_{map} = \frac{1}{N} \Sigma \left| \frac{\left(\frac{dp_f}{dZ}\right)_{pred} - \left(\frac{dp_f}{dZ}\right)_{exp}}{\left(\frac{dp_f}{dZ}\right)_{exp}} \right| x\ 100\% \quad (18)$$

$$E_{rmsp} = \sqrt{\frac{1}{N-1} \Sigma \left(\frac{\left(\frac{dp_f}{dZ}\right)_{pred} - \left(\frac{dp_f}{dZ}\right)_{exp}}{\left(\frac{dp_f}{dZ}\right)_{exp}} \right)^2} x\ 100\% \quad (19)$$

The results of pressure gradient calculations using the C value proposed by Kawahara et al. (2011) and Mishima and Hibiki (1996) are shown in Figure 7.

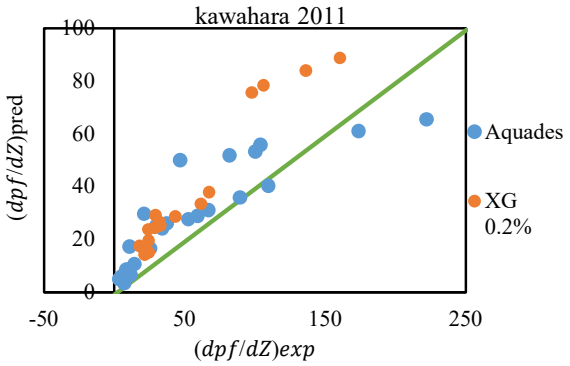

(a)

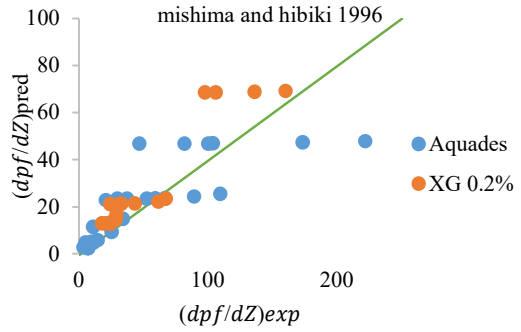

(b)

Figure 7. Comparison of pressure gradient calculation with experiment using the formula (a) Kawahara et al. and (b) Mishima and Hibiki

Table 2. Mean error and root mean square error with comparison of the friction multiplier factor of two-phase flow to predict the pressure gradient of two-phase flow

	Fluids	EM (%)	ERMS (%)
Kawahara et al	Aquades	-24.5645	42.72819
	XG 0.2%	-26.8032	30.76041
Mishima dan Hibiki	Aquades	-46.7829	52.8308
	XG 0.2%	-31.8740	38.7272

The figure shows a comparison between the predicted frictional pressure drop gradient (dpf/dz) pred and the experimental measurement results (dpf/dz) exp for two types of fluids, namely distilled water and 0.2% Xanthan Gum (XG) solution. The green line in the graph depicts an ideal line with a slope of 1 (y=x), indicating a perfect prediction where the predicted results are in full agreement with the experimental results. The blue dot data representing distilled water shows a larger variation and is more spread out from this ideal line, indicating that the prediction model is less accurate for this fluid under some conditions. In contrast, the orange dot data for 0.2% XG solution shows a better agreement with the ideal line, although there are some significant deviations at higher values. This indicates that the prediction model is generally more accurate for 0.2% XG solution compared to distilled water. Overall, despite some deviations, the prediction model tends to provide a fairly reasonable estimate of the frictional pressure drop gradient for both fluids, with more accurate predictions for 0.2% XG solution. This figure suggests that the prediction model has varying degrees of success depending on the fluid type and specific conditions, and that there is room for improvement in model accuracy, especially in the higher range of values.

In Table 2, we can see the percentage error data that has been calculated using the formula from Kawahara et al. shows that for distilled water, the EM value is -24% and Erms is 42% and XG 0.2% has an EM value of -26% and Erms is 30%, while using the formula from Mishima and Hibiki, distilled water has an EM value of -46% and Erms is 52% and XG 0.2% has an EM value of -31% and Erms is 38%. From these data, it can be seen that the constant correlation, C the two-phase flow multiplier factor obtained in Figure 4b shows the best agreement with the pressure drop data of the two-phase flow pattern in this study. All tables, images, graphs, diagrams, and schemes.

4. CONCLUSION

This study investigated the two-phase flow characteristics of a mixture of Xanthan Gum (XG) and Nitrogen in a square-shaped horizontal microchannel after heating. Through experimental and numerical approaches, we successfully identified the flow patterns, flow pattern transitions, and frictional pressure drops. Three main patterns were identified: slug, churn, and slug-annular, with no bubbly and wavy-annular patterns in XG solution due to the influence of non-Newtonian viscosity. The flow pattern transitions showed a strong dependence on the gas flow rate and XG concentration, which affected the slug morphology. The pressure drop prediction model showed a better accuracy level in 0.2% XG solution compared to distilled water, with the error value still within acceptable limits. These findings emphasize the importance of the influence of fluid rheological properties on two-phase flow dynamics and contribute to the development of micro-cooling systems and other microfluidic applications more efficiently. Overall, this study provides valuable insights into the dynamics of two-phase flow at the microscale and provides a solid foundation for the development of more advanced and practical microfluidic technologies.

REFERENCE

[1] S. G. Kandlikar, “Nucleation characteristics and stability considerations during flow boiling in microchannels,” *Exp. Therm. Fluid Sci.*, vol. 30, no. 5, 2006, doi: 10.1016/j.expthermflusci.2005.10.001. https://doi.org/10.1016/j.expthermflusci.2005.10.001

[2] Y. K. Prajapati, M. Pathak, and M. K. Khan, “Transient heat transfer characteristics of segmented finned microchannels,” *Exp. Therm. Fluid Sci.*, vol. 79, 2016, doi: 10.1016/j.expthermflusci.2016.07.004. https://doi.org/10.1016/j.expthermflusci.2016.07.004

[3] H. Wang, Y. Yang, M. He, and H. Qiu, “Subcooled flow boiling heat transfer in a microchannel with chemically patterned surfaces,” *Int. J. Heat Mass Transf.*, vol. 140, 2019, doi:

10.1016/j.ijheatmasstransfer.2019.06.027. https://doi.org/10.1016/j.ijheatmasstransfer.2019.06.027

[4] M. H. Mansour, A. Kawahara, and M. Sadatomi, "Experimental investigation of gas-non-Newtonian liquid two-phase flows from T-junction mixer in rectangular microchannel," *Int. J. Multiph. Flow*, vol. 72, 2015, doi: 10.1016/j.ijmultiphaseflow.2015.02.019. https://doi.org/10.1016/j.ijmultiphaseflow.2015.02.019

[5] K. Feng and H. Zhang, "Pressure drop and flow pattern of gas-non-Newtonian fluid two-phase flow in a square microchannel," *Chem. Eng. Res. Des.*, vol. 173, 2021, doi: 10.1016/j.cherd.2021.07.010. https://doi.org/10.1016/j.cherd.2021.07.010

[6] Q. Lv, T. Yan, Y. Feng, H. Huang, and J. Qin, "Experimental and numerical study of flow boiling heat transfer characteristics in rectangular groove-wall microchannels," *Int. J. Heat Mass Transf.*, vol. 220, 2024, doi: 10.1016/j.ijheatmasstransfer.2023.124999. https://doi.org/10.1016/j.ijheatmasstransfer.2023.124999

[7] A. Kawahara, Y. Yonemoto, and Y. Arakaki, "Pressure Drop for Gas and Polymer Aqueous Solution Two-Phase Flows in Horizontal Circular Microchannel," *Flow, Turbul. Combust.*, vol. 105, no. 4, 2020, doi: 10.1007/s10494-020-00127-z. https://doi.org/10.1007/s10494-020-00127-z

[8] J. W. S. G. Coleman, "Characterization of two-phase flow patterns in small diameter round and rectangular tubes," *Int. J. Heat Mass Transf.*, vol. 14, no. 15, pp. 2869–2881, 1999, doi: DOI:10.4028/https://doi.org/10.1016/S0017-9310(98)00362-7. https://doi.org/10.1016/S0017-9310(98)00362-7

[9] T. Zhang, B. Cao, Y. Fan, Y. Gonthier, L. Luo, and S. Wang, "Gas-liquid flow in circular microchannel. Part I: Influence of liquid physical properties and channel diameter on flow patterns," *Chem. Eng. Sci.*, vol. 66, no. 23, 2011, doi: 10.1016/j.ces.2011.07.035. https://doi.org/10.1016/j.ces.2011.07.035

[10] P. Yang, Y. Zhang, X. Wang, and Y. wen Liu, "Heat transfer measurement and flow regime visualization of two-phase pulsating flow in an evaporator," *Int. J. Heat Mass Transf.*, vol. 127, 2018, doi: 10.1016/j.ijheatmasstransfer.2018.08.065. https://doi.org/10.1016/j.ijheatmasstransfer.2018.08.065

[11] A. Ilinca *et al.*, "Fluid-flow pressure measurements and thermo-fluid characterization of a single loop two-phase passive heat transfer device," in *Journal of Physics: Conference Series*, 2017. doi: 10.1088/1742-6596/923/1/012022. https://doi.org/10.1088/1742-6596/923/1/012022

[12] Z. C. Yang, Q. C. Bi, B. Liu, and K. X. Huang, "Nitrogen/non-Newtonian fluid two-phase upward flow in non-circular microchannels," *Int. J. Multiph. Flow*, vol. 36, no. 1, 2010, doi: 10.1016/j.ijmultiphaseflow.2009.07.011. https://doi.org/10.1016/j.ijmultiphaseflow.2009.07.011

[13] W. Kozicki, C. H. Chou, and C. Tiu, "Non-Newtonian flow in ducts of arbitrary cross-sectional shape," *Chem. Eng. Sci.*, vol. 21, no. 8, 1966, doi: 10.1016/0009-2509(66)80016-7. https://doi.org/10.1016/0009-2509(66)80016-7

[14] A. I. Ageev and A. N. Osiptsov, "Pulsating Flow of a Viscous Fluid over a Cavity Containing a Compressible Gas Bubble," *Fluid Dyn.*, vol. 56, no. 6, 2021, doi: 10.1134/S001546282106001X. https://doi.org/10.1134/S001546282106001X

[15] A. Kawahara, M. Sadatomi, K. Nei, and H. Matsuo, "Characteristics of two-phase flows in a rectangular microchannel with a T-junction type gas-liquid mixer," in *Heat Transfer Engineering*, 2011. doi: 10.1080/01457632.2010.509752. https://doi.org/10.1080/01457632.2010.509752

[16] K. Mishima and T. Hibiki, "Some characteristics of air-water two-phase flow in small diameter vertical tubes," *Int. J. Multiph. Flow*, vol. 22, no. 4, 1996, doi: 10.1016/0301-9322(96)00010-9. https://doi.org/10.1016/0301-9322(96)00010-9

[17] D. Chisholm, "A theoretical basis for the Lockhart-Martinelli correlation for two-phase flow," *Int. J. Heat Mass Transf.*, vol. 10, no. 12, 1967, doi: 10.1016/0017-9310(67)90047-6. https://doi.org/10.1016/0017-9310(67)90047-6